Thermoreflectance in Semiconductors*

E. MATATAGUI,† A. G. THOMPSON, AND MANUEL CARDONA‡
Physics Department, Brown University, Providence, Rhode Island 02912
(Received 25 June 1968)

The thermoreflectance spectra of Si, AlSb, GaP, GaAs, GaSb, InP, InAs, InSb, ZnO, ZnS, ZnSe, ZnTe, CdS, CdSe, CdTe, HgSe, and HgTe are reported. Measurements were made on most materials at both room and liquid-nitrogen temperatures. The positions of the peaks observed are compared with previous reflectance and electroreflectance data. Some representative spectra were subjected to a Kramers-Kronig analysis, and the changes in the real and imaginary parts of the dielectric constant, induced by the change in temperature of the sample, were obtained. The resulting line shapes are compared with those derived from elementary theory. In order to achieve reasonable agreement between theory and experiment, it is found necessary to invoke the presence of excitons at all the interband edges. It is demonstrated that, under certain conditions, the type of critical point involved in the transition can be identified.

I. INTRODUCTION

THE measurement of the reflectance of semiconductors at energies higher than the fundamental edge has proved very useful in studying the band structures of these materials.[1,2] More recently, modulation techniques have been employed for the same purpose, yielding greater sensitivity and resolution. These techniques rely on the periodic perturbation of a parameter which affects the optical properties of the semiconductor, such as an electric field (electroreflectance,[3,4] electroabsorption[5]), stress (piezoreflectance,[6–8] piezoabsorption[9,10]), etc.

Electroreflectance is probably the easiest of all optical modulation techniques from the experimental point of view. The detailed interpretation of the results is hampered, however, by the fact that the modulating field destroys the translational invariance along its direction. While there is no question that sharp structure appears only close to critical points, theory has so far failed to account quantitatively for many of the observed line shapes. Piezoreflectance experiments are simpler from the theoretical point of view since translational symmetry is not destroyed; the line shapes in the neighborhood of critical points should just be the derivatives of the line shapes of the unmodulated spectra. Unfortunately, this theoretical simplicity is not shared by its experimental realization and, so far, piezoreflectance measurements have not given line shapes above the fundamental energy gap that could be quantitatively interpreted.

In view of these difficulties, inherent to optical experiments in which the properties of the sample are modulated, the desirability of wavelength-modulation experiments[11–13] becomes apparent. Their theoretical interpretation should be very simple since it involves only the theory of the optical constants of the material, and not that of the effect of the modulating perturbation on such optical constants. However, wavelength modulation is not simple from the experimental standpoint. In a conventional single-beam experiment, not only the derivative spectrum of the sample is obtained, but also that of the incident beam I_0. Elimination of the derivative of I_0 requires a carefully compensated double-beam system[14] which is difficult to build and to operate.

In view of the above discussion, the possible use of temperature modulation as an alternative to wavelength modulation should be considered. The effect of an increase in temperature on the optical properties of the sample is to shift the energy gaps, which is equivalent to wavelength modulation, and to broaden the critical point involved. The shift of an energy gap has two components, one due to thermal expansion and another due to the electron-phonon interaction. The thermal-expansion shift is of the same sign as the phonon shift for most critical points observed, and of comparable magnitude. The broadening is due only to the electron-phonon interaction, and the effects are small compared to the total shift (see Sec. II). Under this assumption, subject to experimental confirmation, thermal- and wavelength-modulation spectra should be

* Work supported by the Advanced Research Projects Agency and the U. S. Army Research Office (Durham).
† Fellow, Consejo Nacional de Investigaciones Cientificas y Tecnicas, Argentina.
‡ Alfred P. Sloan Foundation Research Fellow.
[1] M. Cardona, in *Proceedings of the International Conference on the Physics of Semiconductors, Paris, 1964* (Academic Press Inc., New York, 1965), p. 181.
[2] J. C. Phillips, in *Solid State Physics*, edited by F. Seitz and D. Turnbull (Academic Press Inc., New York 1966), Vol. 18, p. 56.
[3] B. O. Seraphin and N. Bottka, Phys. Rev. **145**, 628 (1966).
[4] M. Cardona, K. L. Shaklee, and F. H. Pollak, Phys. Rev. **154**, 696 (1967).
[5] A. Frova, P. Handler, F. A. Germano, and D. E. Aspnes, Phys. Rev. **145**, 575 (1967).
[6] W. E. Engeler, H. Fritsche, M. Garfinkel, and J. J. Tiemann, Phys. Rev. Letters **14**, 1069 (1965).
[7] G. W. Gobeli and E. O. Kane, Phys. Rev. Letters **15**, 142 (1965).
[8] U. Gerhardt, D. Beaglehole, and R. Sandrock, Phys. Rev. Letters **19**, 309 (1967).
[9] I. Balslev, Phys. Letters **24A**, 113 (1967).
[10] W. E. Engeler, M. Garfinkel, and J. J. Tiemann, Phys. Rev. **155**, 693 (1967).
[11] I. Balslev, Phys. Rev. **143**, 636 (1966).
[12] R. E. Drews, Bull. Am. Phys. Soc. **12**, 384 (1967).
[13] K. L. Shaklee, J. E. Rowe, and M. Cardona, Phys. Rev. **174**, 144 (1968), and references therein.
[14] K. L. Shaklee, Ph.D. thesis, Brown University, 1968 (unpublished).

equivalent except for scaling factors related to the temperature coefficients of the various gaps.

Thermoreflectance measurements have been made by Batz on Ge,[15,16] by Lange and Henrion on CdS and Se,[17] on graphite by Balzarotti and Grandolfo,[18] on Au [19] and Ni [20] by Scouler and co-workers, and on the alkali metals by Matatagui and Cardona.[21] Thermoabsorption measurements at the fundamental edge have been made by Berglund[22] on Si, GaAs, CdS, and $KTaO_3$.

We have applied the method of thermoreflectance, at temperatures between 80 and 300°K, to materials having the diamond (Si), zinc-blende (AlSb, GaP, GaAs, GaSb, InP, InAs, InSb, ZnS, ZnSe, ZnTe, CdTe, HgSe, and HgTe) and wurtzite (ZnO, CdS, and CdSe) structures. The results are compared with those found previously from reflectance and electroreflectance measurements. Representative spectra are transformed into changes in the real and imaginary parts of the dielectric constant by means of a Kramers-Kronig analysis. These derived spectra are then compared with theory in an attempt to identify the critical points responsible for the transitions.

II. THEORY OF THERMOREFLECTANCE

The relation between the energy band structure and the optical properties of the semiconductors under consideration has been described previously.[4] Briefly, five sets of transitions are observed in the typical range of modulation experiments (1–6 eV); we denote these sets by E_0, E_1, E_0', E_2, and E_1' (see Fig. 1).

(i) E_0, $E_0+\Delta_0$: a spin-orbit-split doublet associated with the lowest direct gap at $\mathbf{k}=0$. Δ_0 is the splitting of the corresponding valence-band state (Γ_{15}).

(ii) E_1, $E_1+\Delta_1$: a spin-orbit-split doublet which has been quite conclusively identified to be due to critical points in the {111} directions (Λ). These critical points are of the M_1 variety (saddle points), and there may be, nearly degenerate with them, a pair of M_0 critical points at L.

(iii) E_0', $E_0'+\Delta_0'$, and possibly others: a cluster of critical points in the vicinity of the Γ_{15v}-Γ_{15c} gap. These critical points are most likely to occur at $\mathbf{k}=0$ and in the {100} directions (Δ) close to $\mathbf{k}=0$.

(iv) E_2, $E_2+\delta$, $E_2+\Delta_2$: a cluster of critical points nearly degenerate with the ($X_{5v}\rightarrow X_1$, X_3) gap. Such critical points occur at a number of high- and low-symmetry directions (e.g., Σ, U[23,24]), but it is usually assumed that δ is the X_1-X_3 splitting, while Δ_2 is the spin-orbit splitting of X_5.

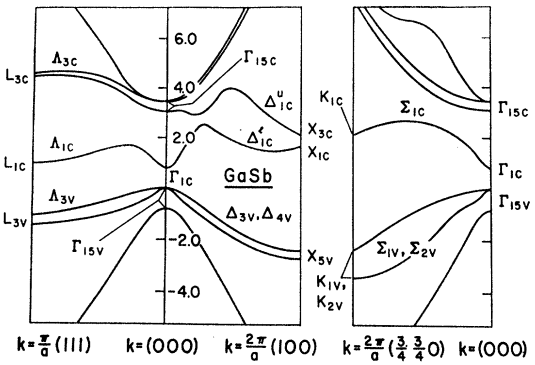

FIG. 1. Band structure of GaSb derived by the $\mathbf{k}\cdot\mathbf{p}$ method (see Ref. 24).

(v) E_1', $E_1'+\Delta_1'$, and others: a quadruplet due to $L_{3v}\rightarrow L_{3c}$ critical points which arises from the spin-orbit splittings of L_{3v} and L_{3c}. This structure is observed only for a few low-band-gap materials in modulation experiments because of the above spectral limitation.

As is well known, the singular behavior of the dielectric constant in the vicinity of a three-dimensional allowed critical point is given by

$$\epsilon \propto b(\omega-\omega_g)^{1/2}, \tag{1}$$

where the constant b is equal to i^{r+1} in the vicinity of of an M_r critical point. Broadening, essential for the treatment of temperature modulation, has been neglected in Eq. (1). It is possible to introduce broadening in the expression in a phenomenological manner by replacing the frequency ω by $\omega+i\Gamma$, where Γ is positive (Lorentzian broadening[16]). By making this substitution in Eq. (1) and separating the real and imaginary parts in the resulting square-root, we obtain

$$\epsilon \propto b\{\omega-\omega_g+[(\omega-\omega_g)^2+\Gamma^2]^{1/2}\}^{1/2} +ib\{\omega_g-\omega+[(\omega-\omega_g)^2+\Gamma^2]^{1/2}\}^{1/2}. \tag{2}$$

This equation can be written in a simpler form by using instead of the frequency ω the reduced variable $x=(\omega-\omega_g)/\Gamma$. Then

$$\epsilon \propto b\Gamma^{1/2}\{[x+(x^2+1)^{1/2}]^{1/2}+i[-x+(x^2+1)^{1/2}]^{1/2}\} =b\Gamma^{1/2}[\Phi(x)+i\Phi(-x)], \tag{3}$$

with $\Phi(x)=[x+(x^2+1)^{1/2}]^{1/2}$.

As mentioned earlier, a temperature-modulation spectrum consists of a combination of the derivative of ϵ with respect to ω (or ω_g) and the derivative with respect to the broadening parameter Γ. Both derivatives can be obtained[16] from Eq. (3) in terms of the function

[15] B. Batz, Solid State Commun. **4**, 241 (1966).
[16] B. Batz, Solid State Commun. **5**, 985 (1967).
[17] H. Lange and W. Henrion, Phys. Status Solidi **23**, K67 (1967).
[18] A. Balzarotti and M. Grandolfo, Phys. Rev. Letters **20**, 9 (1968).
[19] W. J. Scouler, Phys. Rev. Letters **18**, 445 (1967).
[20] J. Hanus, J. Feinleib, and W. J. Scouler, Phys. Rev. Letters **19**, 16 (1967).
[21] E. Matatagui and M. Cardona, Solid State Commun. **6**, 313 (1968).
[22] C. N. Berglund, J. Appl. Phys. **37**, 3019 (1966).
[23] E. O. Kane, Phys. Rev. **146**, 558 (1966).
[24] C. W. Higginbotham, F. H. Pollak, and M. Cardona, in Proceedings of the International Conference on the Physics of Semiconductors, Moscow, 1968 (unpublished).

$F(x)=2d\Phi/dx$:

$$d\epsilon/d\omega \propto \tfrac{1}{2}b\Gamma^{-1/2}[F(x)-iF(-x)], \quad (4a)$$

$$d\epsilon/d\Gamma \propto \tfrac{1}{2}b\Gamma^{-1/2}[F(-x)+iF(x)], \quad (4b)$$

where

$$F(x)=(x^2+1)^{-1/2}[(x^2+1)^{1/2}+x]^{1/2}. \quad (4c)$$

The line shapes of $d\epsilon_r$ and $d\epsilon_i$ with respect to ω and Γ represented by Eqs. (4) are shown in Fig. 2 for the four types of three-dimensional critical points. In order to obtain the experimental thermoreflectance lines, Eqs. (4a) and (4b) must be multiplied by $d\omega/dT(=-d\omega_g/dT)$ and $d\Gamma/dT$, respectively. The coefficient $d\omega_g/dT$ can, in principle, be either positive or negative, but is known to be negative for all the structure discussed here. Its value is typically -4×10^{-4} eV $(°C)^{-1}$.[25-27] The coefficient $d\Gamma/dT$ is necessarily positive, and it is expected to be approximately equal to the Boltzmann constant ($\sim10^{-4}$ eV $(°C)^{-1}$); this expectation is borne out by conventional optical measurements made as a function of temperature.[28]

The considerations given above have been limited to transitions between one-electron energy bands. Of the several types of many-body corrections, exciton effects (e.g., the Coulomb interaction between an excited electron and the hole left behind) are known to affect significantly the one-electron optical constants in the neighborhood of critical points.[2] The Coulomb interaction yields[29] bound exciton states below the lowest direct gap E_0. The quantitative treatment of the exciton interaction at critical points above the lowest gap, and in particular at hyperbolic critical points (M_1 and M_2), is a difficult theoretical problem.[30,31]

Toyozawa *et al.*[32] have treated this problem by replacing the Coulomb potential by a finite-range potential. They have shown that the effect of such a potential on the singular line shapes ($\Gamma=0$) in the vicinity of a critical point M_r is to mix the M_r line shapes with those one would expect for an M_{r+1} critical point (one defines $M_4\equiv M_0$). This type of treatment can also be applied to the Lorentzian-broadened one-electron line shapes of Fig. 2. While this analysis does not yield the bound exciton states below E_0, it should represent quite well the experimental line shapes provided that enough broadening is present so as to make the bound states merge with the continuum ($\Gamma\sim$exciton binding energy). This condition holds for all the III-V compounds measured for temperatures above 77°K.

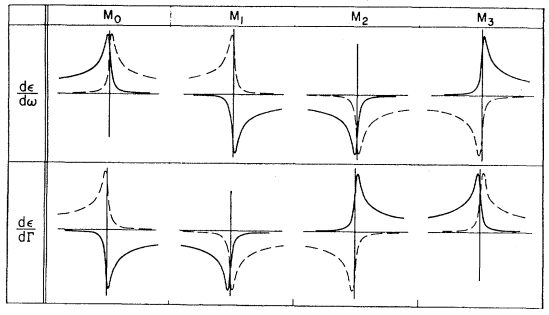

FIG. 2. The derivatives of ϵ_r(—) and ϵ_i(- - -) with respect to the frequency ω and the Lorentzian broadening parameter Γ for the four types of three-dimensional broadened critical points, derived from Eqs. (4).

If discrete exciton states are distinctly present, one can obtain the thermal-modulation line shapes with the phenomenological Lorentzian expression for the exciton dispersion[33]:

$$\epsilon\sim(1-2iA)/[(\omega_{ex}-\omega)-i\Gamma]. \quad (5)$$

In Eq. (5), A is an asymmetric broadening parameter (usually small), Γ is the Lorentzian broadening parameter, and ω_{ex} is the energy at which the exciton bound state occurs. Figure 3 shows the derivatives of ϵ_r and ϵ_i with respect to ω and Γ obtained from Eq. (5) for $A=0$. The effect of asymmetric broadening ($A\neq0$) is to mix the ϵ_r and ϵ_i line shapes.

The Kramers-Kronig analysis used to find the changes in the optical constants due to the temperature modulation is similar to that used in Ref. 4. The normal-incidence reflectance R is expressed in terms of n, k, and the phase θ.

$$e^{i\theta}R^{1/2}=(n+ik-1)/(n+ik+1).$$

Then

$$\begin{aligned}\Delta\epsilon_r&=\tfrac{1}{2}n(n^2-3k^2-1)\Delta R/R+k(3n^2-k^2-1)\Delta\theta,\\ \Delta\epsilon_i&=\tfrac{1}{2}k(3n^2-k^2-1)\Delta R/R+n(3k^2-n^2-1)\Delta\theta,\\ \Delta\theta(E_0)&=\frac{E_0}{\pi}\int_0^\infty\frac{\Delta R/R-\Delta R_0/R_0}{E^2-E_0^2}dE.\end{aligned} \quad (6)$$

The optical constants n and k were obtained from a Kramers-Kronig analysis of reflectance data[34,35] and the integration was performed with a five-point formula and 0.01-eV mesh, adequate for the data presented here. Thus a comparison between the $\Delta\epsilon_r$ and $\Delta\epsilon_i$ curves and Figs. 2 and 3 can be made directly.

III. EXPERIMENTAL LAYOUT

(a) Optical. Light from a high-pressure xenon arc or a quartz-iodine tungsten-filament lamp was focused on the entrance slit of a Bausch & Lomb 50-cm grating monochromator. The resulting monochromatic light

[25] M. Cardona and G. Harbeke, J. Appl. Phys. **34**, 813 (1963), and references therein.
[26] M. Cardona and D. L. Greenaway, Phys. Rev. **131**, 98 (1963).
[27] A. G. Thompson and J. C. Woolley, Can. J. Phys. **44**, 2927 (1966).
[28] M. Cardona and H. S. Sommers, Phys. Rev. **122**, 1382 (1961).
[29] R. J. Elliot, Phys. Rev. **108**, 1384 (1957).
[30] C. Duke and B. Segall, Phys. Rev. Letters **17**, 19 (1966).
[31] B. Velický and J. Sak, Phys. Status Solidi **16**, 147 (1966).
[32] Y. Toyozawa, M. Inoue, T. Inoui, M. Okazaki, and E. Hanamura, Proc. Phys. Soc. Japan Suppl. **21**, 133 (1967).
[33] Y. Toyozawa, Progr. Theoret. Phys. (Kyoto) **20**, 53 (1958).
[34] H. R. Philipp and H. Ehrenreich, Phys. Rev. **129**, 1550 (1963).
[35] M. Cardona, J. Appl. Phys. **36**, 2181 (1965).

was focused on the sample, reflected at near-normal incidence, and refocused on an EMI 6256B or a Dumont 6911 photomultiplier for the ultraviolet/visible and near-infrared regions, respectively. A resolution of 15 Å or better was used, depending on the sample and spectral region.

(b) Electronics. A block diagram of the experimental apparatus is shown in Fig. 4; it is similar to that used earlier for electroreflectance experiments.[4] The photomultiplier current consists of a dc signal proportional to the reflectance of the sample R, and an ac signal proportional to the modulated change in reflectance ΔR caused by the periodic temperature variation of the sample. The ac portion is detected by a PAR HR-8 lock-in amplifier, the output of which is displayed on the Y axis of an X-Y recorder. The dc portion is kept constant at a known value by varying the photomultiplier power-supply voltage with a servomechanism; hence the Y-axis reading is proportional to the ratio $\Delta R/R$. A voltage proportional to the energy $h\nu$ of the monochromatic radiation, obtained from a potentiometer

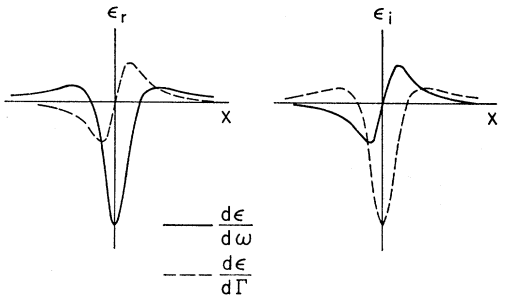

FIG. 3. The derivatives of ϵ_r(—) and ϵ_i(- - -) with respect to the frequency and the Lorentzian broadening parameter Γ for an exciton at an M_0 critical point, according to Eq. (5) with $A=0$.

corrected to the wavelength drive of the monochromator and a battery, is supplied to the X axis of the recorder.

A square-wave generator supplies power to heat the sample and the reference voltage for the lock-in amplifier. The frequency used was a compromise between signal strength and noise level, and usually lay between 10 and 30 Hz.

(c) Sample preparation. In order to keep the heat capacity of the sample as small as possible and still maintain an adequate surface area off which to reflect the light, the samples were ground down to 100–400-μ thickness, and were typically 5–10 mm long by 2–3 mm wide. The back surface was left rough from the lapping process, while the front surface was either cleaved whenever possible or else mechanically polished with diamond paste and then etched. One material, CdS, was available in the form of vapor-grown platelets, and these were used with no further treatment.

(d) Sample mounting. The thin sample was mounted on a sapphire heat sink. If the sample was conducting, contacts were soldered or diffused into it, leads attached

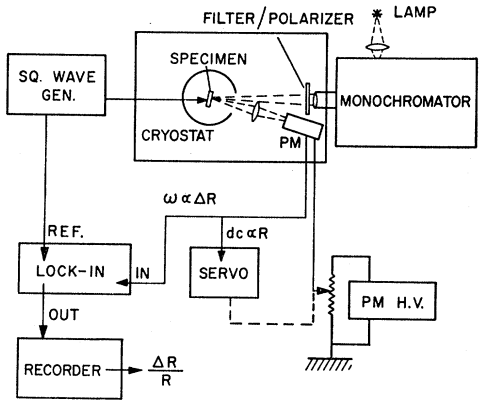

FIG. 4. Experimental setup used for thermoreflectance studies.

for supplying the current, and a thin film of silicone vacuum grease or GE varnish used to bond it to the heat sink. Nonconducting samples were bonded to the heat sink with silver paint (GE No. 4817) which was used as the indirect heater. A separate heating strip, insulated from the sample, gave similar results to the above two methods; hence the spectra obtained were due to temperature modulation, and not to some other process. The heat sink was mounted on the copper cold finger of a simple metal cryostat fitted with a Suprasil window. A vacuum of approximately 10^{-6} Torr was maintained inside the cryostat while coolants such as liquid nitrogen (77°K), dry ice+acetone (~200°K), or ice+water (273°K) were added to the reservoir above the cold finger.

The dc temperature rise of the sample was measured with a thermocouple attached to its surface, but away from the incident light beam. For small samples the temperature rise was estimated from the results and a knowledge of temperature coefficients from reflectance and absorption measurements.[25–27] The magnitude of the temperature modulation was difficult to measure directly with our experimental arrangement. However, it can be estimated from a knowledge of the limiting value of $\Delta R/R$ below the fundamental edge. From $R=[(1-n)/(1+n)]^2$ we calculate

$$\Delta R/R=[4n/(n^2-1)]\Delta n/n. \quad (7)$$

The values of dn/dT have been measured for several materials by Cardona.[36] Using these values and estimating others we obtain modulations ~2°C for most of our samples.

IV. RESULTS

In this section all comparisons with electroreflectance results are made with the data of Ref. 4 unless otherwise stated.

Diamond structure: Si. Thermoreflectance spectra at

[36] M. Cardona, in *Proceedings of the International Conference on Semiconductor Physics, 1960* (Czechoslovakian Academy of Sciences, Prague, 1961), p. 388.

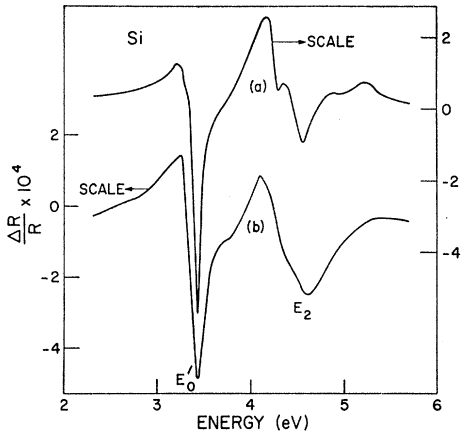

FIG. 5. Thermoreflectance spectrum of Si at (a) liquid-nitrogen temperature and (b) room temperature.

room and low (slightly above 77°K, as discussed in Sec. III) temperatures are shown in Fig. 5. The dominant structure is the E_0' and E_2 peaks. The low-temperature spectrum shows the main E_0' peak at 3.43 eV with a shoulder around 3.32 eV. These two peaks correspond to the peaks observed by Seraphin[37] in the low-temperature (95°K) electroreflectance spectrum at 3.42 and 3.34 eV. The shoulder in the thermoreflectance is relatively weaker than the corresponding electroreflectance structure, and this is attributed to the small temperature coefficient of the lower-energy peak. The 3.32–3.43-eV splitting can also be seen in the unmodulated reflectance at low temperature.[38]

The low-temperature spectrum shows the E_2 peak at 4.55 eV and a smaller peak 0.25 eV lower in energy.

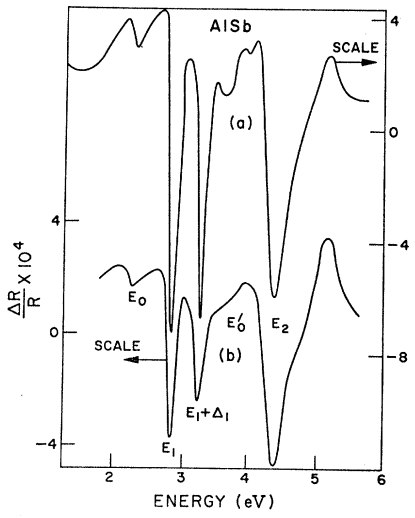

FIG. 6. Thermoreflectance spectrum of AlSb at (a) liquid-nitrogen temperature and (b) room temperature.

[37] B. O. Seraphin, Phys. Rev. **140**, A1716 (1965).
[38] R. A. Forman, D. E. Aspnes, and M. Cardona (to be published).

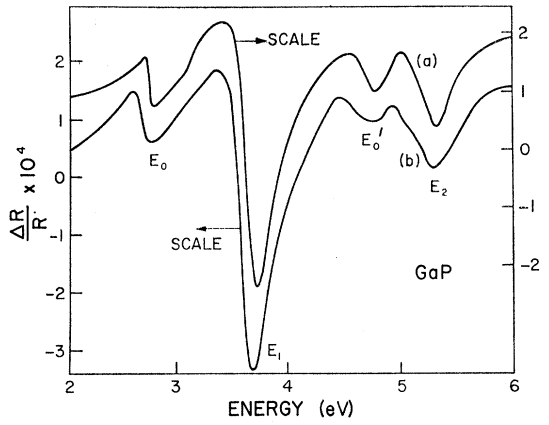

FIG. 7. Thermoreflectance spectrum of GaP at (a) liquid-nitrogen temperature and (b) room temperature.

At room temperature the latter appears only as a shoulder. This structure has been observed in reflectance[39] and electroreflectance. Some structure possibly associated with E_1' appears at higher energies but is too weak for a positive identification.

Zinc-blende structure: AlSb. See Fig. 6. The low-temperature spectrum shows a small peak at 2.32 eV attributed to E_0. The two large peaks at 2.86 and 3.29 eV correspond to E_1 transitions, while small peaks at 3.7 and 4.0 eV correspond to E_0' and $E_0'+\Delta_0'$. E_2 transitions are responsible for the large peak at 4.4 eV. The room-temperature spectrum shows similar structure, and in addition a shoulder at $\sim$4.7 eV is probably due to $E_2+\delta$ transitions. All peak positions and splittings agree well with the electroreflectance results.

GaP. See Fig. 7. Both room- and low-temperature spectra are similar. The E_0 edge appears as small structure around 2.8 eV, which is broad enough to mask the expected Δ_0 splitting of $\sim$0.1 eV. The large peak at 3.7 eV has been attributed[40] to E_1 transitions, while the peaks at 4.8 and 5.3 eV have been attributed to E_0'

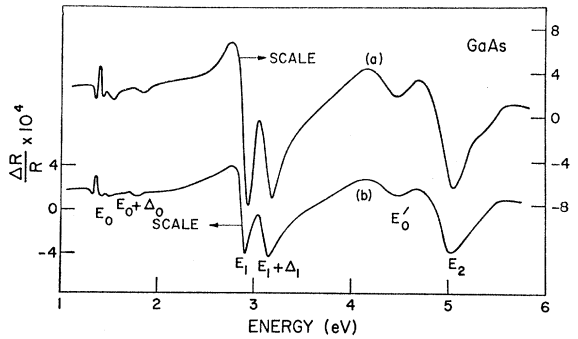

FIG. 8. Thermoreflectance spectrum of GaAs at (a) liquid-nitrogen temperature and (b) room temperature.

[39] F. Lukeš and E. Schmidt, in *Proceedings of the International Conference on the Physics of Semiconductors, Paris, 1964* (Academic Press Inc., New York, 1965), p. 197.
[40] A. G. Thompson, M. Cardona, K. L. Shaklee, and J. C. Woolley, Phys. Rev. **146**, 601 (1966).

and E_2 transitions, respectively. Since both Δ_1 and Δ_0' are small in this material, the E_1 and E_0' peaks are broad enough to mask the expected splitting.

GaAs. See Fig. 8. E_0 and $E_0+\Delta_0$ edges are attributed to the structure occurring at 1.46 and 1.80 eV in the low-temperature spectrum. The doublet at 2.95 and 3.19 eV agrees well with electroreflectance results for the E_1 transitions. The peak at 4.5 eV is attributed to E_0', and a small shoulder at the base of the large E_2 peak is probably caused by $E_0'+\Delta_0'$ transitions; its energy of 4.8 eV compares well with electroreflectance results.[40] The large peak at 5.05 eV is due to E_2 transitions, while a shoulder some 0.3 eV higher is probably due to $E_2+\delta$ transitions.

GaSb. See Fig. 9. The doublet at 2.13 and 2.60 eV in the low-temperature spectrum is attributed to E_1 and $E_1+\Delta_1$ transitions. The three small peaks at $\sim$3.2, 3.6(5), and 3.8 eV are caused by E_0' transitions.[24] The large peak at 4.4 eV is due to E_2 transitions. The room-temperature spectrum shows evidence of a shoulder some 0.35 eV higher than the E_2 peak which is probably caused by $E_2+\delta$ transitions.

InP. See Fig. 10. The E_0 and $E_0+\Delta_0$ transitions are

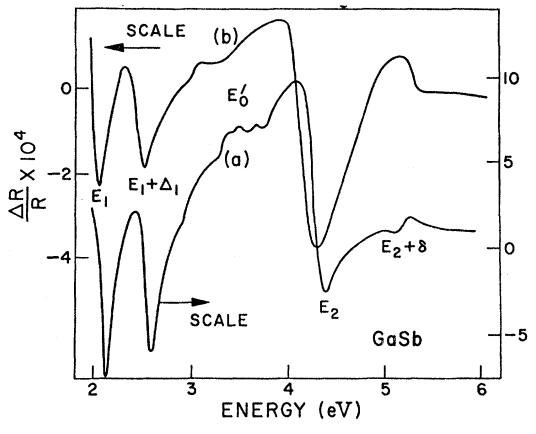

FIG. 9. Thermoreflectance spectrum of GaSb at (a) liquid-nitrogen temperature and (b) room temperature.

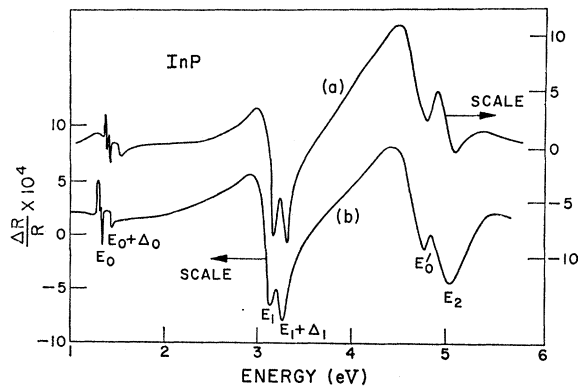

FIG. 10. Thermoreflectance spectrum of InP at (a) liquid-nitrogen temperature and (b) room temperature.

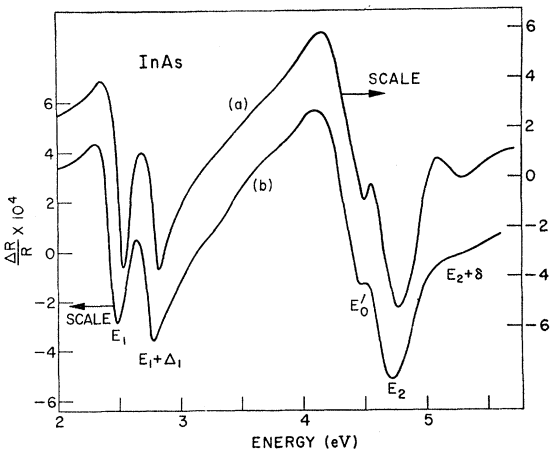

FIG. 11. Thermoreflectance spectrum of InAs at (a) liquid-nitrogen temperature and (b) room temperature.

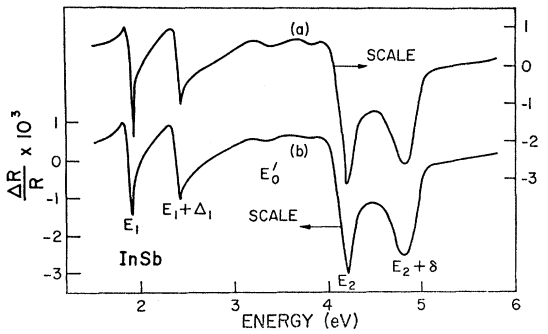

FIG. 12. Thermoreflectance spectrum of InSb at (a) liquid-nitrogen temperature and (b) acetone-plus-dry-ice temperature.

responsible for the structure at around 1.4 eV in both the room- and low-temperature spectra. Unlike electroreflectance, this technique gives results clearly showing the split-off component, and the splitting $\Delta_0=0.10$ eV confirms the tentative electroreflectance result. The small peak lying $\sim$0.02 eV below the main E_0 peak is probably caused by an impurity level; impurity effects have also been seen in the electroreflectance of InP. The doublet around 3.2 eV becomes clearer on cooling; at the same time the splitting increases from 0.12 eV at room temperature to 0.13 eV at liquid-nitrogen temperatures. Line-shape effects and insufficient resolution may be responsible for the discrepancy from the value of 0.15 eV obtained by electroreflectance. Peaks at 4.8 and 5.05 eV are attributed to E_0' and E_2 transitions, respectively.

InAs. See Fig. 11. The E_1 and $E_1+\Delta_1$ doublet displays a splitting of 0.29 eV at both room and low temperatures. The small peak at 4.5 eV is attributed to E_0' transitions, while the large peak at 4.8 eV is due to E_2 transitions. The $E_2+\delta$ peak lying $\sim$0.5 eV higher than the E_2 peak is seen only in the low-temperature spectrum.

InSb. See Fig. 12. The distinctly shaped peaks around

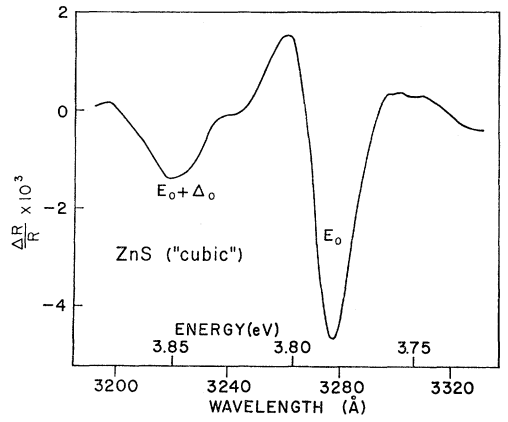

FIG. 13. Thermoreflectance spectrum of ZnS (>95% cubic) at liquid-nitrogen temperature.

2 eV are due to E_1 and $E_1+\Delta_1$ transitions; the splitting $\Delta_1=0.51$ eV agrees well with electroreflectance results. The weak structure at 3.4 and 3.8 eV in the low-temperature spectrum is less well resolved at dry-ice and acetone temperatures, and is probably due to E_0' and $E_0'+\Delta_0'$ transitions, although the peak positions are high when compared with the electroreflectance data. The E_2 and $E_2+\delta$ peaks are strong, and occur at 4.2 and 4.8 eV in the low-temperature spectrum. Some evidence of E_1' transitions is seen at 5.3 eV. These results will be commented on further in Sec. V.

ZnS. See Fig. 13. Results were obtained only at low temperatures. The two main peaks at ~80°K have energies of 3.783 and 3.854 eV and are due to E_0 and $E_0+\Delta_0$ transitions. These energies correspond very closely to reflectance[41] and electroreflectance[42] results; our splitting of 71±4 meV is also in good agreement with that of Refs. 41 and 42. No structure was discernible above the noise level for energies higher than the E_0 structure.

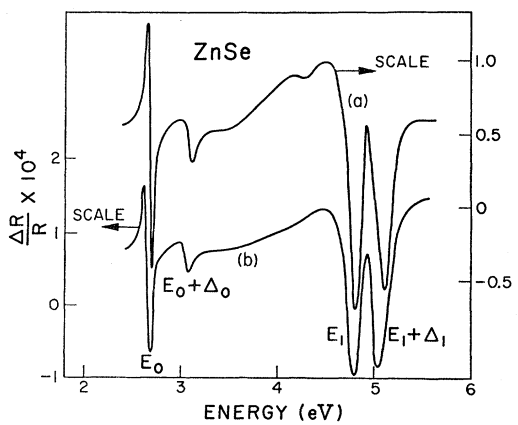

FIG. 14. Thermoreflectance spectrum of ZnSe at (a) liquid-nitrogen temperature and (b) room temperature.

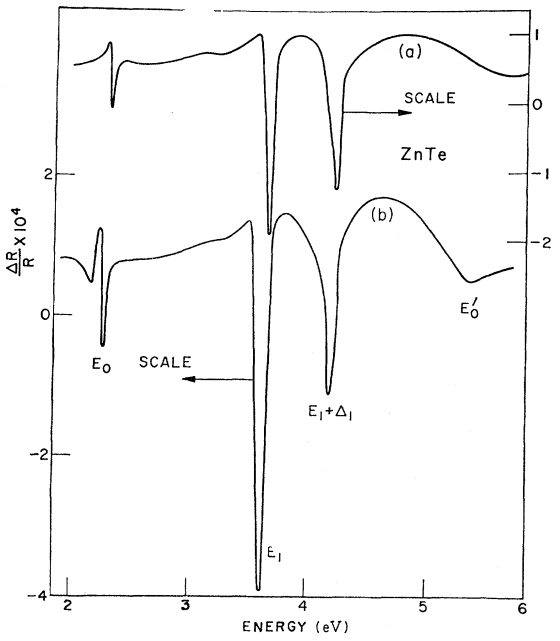

FIG. 15. Thermoreflectance spectrum of ZnTe at (a) liquid-nitrogen temperature and (b) room temperature.

ZnSe. See Fig. 14. The structure around 3 eV is due to E_0 and $E_0+\Delta_0$ transitions; the positions of the edges and the magnitude of the spin-orbit splitting Δ_0 (=0.41 eV) agree well with reflectance data.[1] The doublet occurring at 4.8 and 5.1 eV is caused by E_1 and $E_1+\Delta_1$ transitions.

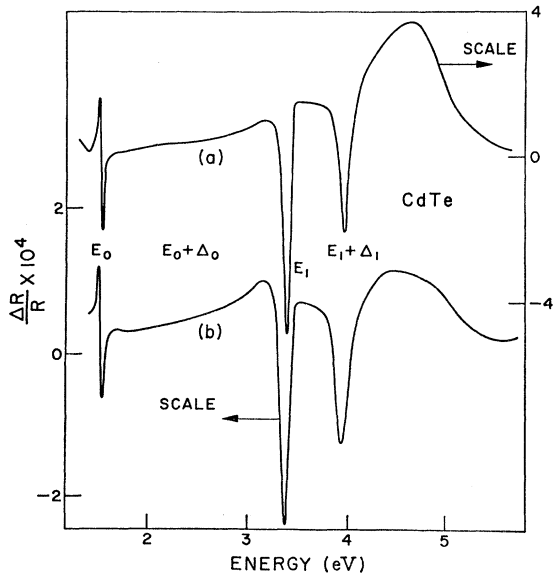

FIG. 16. Thermoreflectance spectrum of CdTe at (a) liquid-nitrogen temperature and (b) room temperature.

[41] J. L. Birman, H. Samelson, and A. Lempicki, G. T. and E. Res. Develop. J. 1, 2 (1961).

[42] R. A. Forman and M. Cardona, in *Proceedings of the International Conference on II-VI Semiconducting Compounds, Providence, 1967*, edited by D. G. Thomas (W. A. Benjamin, Inc., New York, 1968), p. 100.

ZnTe. See Fig. 15. The E_0 edge occurs at 2.28 eV in the low-temperature spectrum. The small structure at ~3.3 eV is possibly due to $E_0+\Delta_0$ transitions. E_1 transitions are responsible for the large doublet around 4 eV having a splitting of 0.57 eV. The peak at 5.3 eV is caused by E_0' transitions. All the positions of the peaks agree well with previous reflectance[1] and electroreflectance data.

CdTe. See Fig. 16. The E_0 edge gives sharp structure at 1.5 eV; weak structure at 2.4 eV, observed only in the low-temperature spectrum, is caused by $E_0+\Delta_0$ transitions. The E_1 and $E_1+\Delta_1$ doublet between 3 and 4 eV has a splitting Δ_1 of 0.56 eV. Some evidence of transitions above 5 eV can be seen, and these will be discussed in Sec. V.

HgSe. See Fig. 17. Broad structure was obtained for this compound—a similar situation occurred in electroreflectance measurements. The doublet centered at 3 eV is split by 0.28 eV, and is due to E_1 and $E_1+\Delta_1$

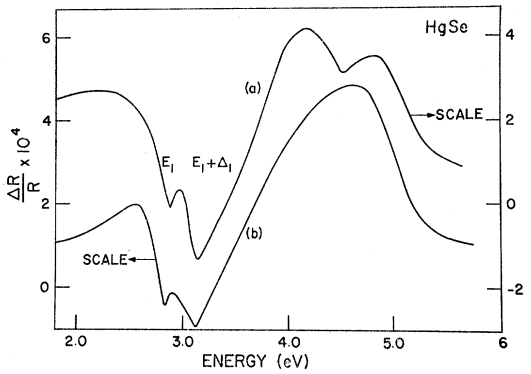

FIG. 17. Thermoreflectance spectrum of HgSe at (a) liquid-nitrogen temperature and (b) room temperature.

transitions. The slight shoulder observed at ~5.1 eV corresponds to E_0' transitions. The peak at 4.5 eV, which is observed only in the low-temperature spectrum, does not seem to correspond to any known transitions.

HgTe. See Fig. 18. The E_1 and $E_1+\Delta_1$ doublet exhibits a splitting of 0.64 eV, and displays a quite distinct line shape (compare with InSb in Fig. 12, and see comments in Sec. V). Weak structure just above 4 eV is due to E_0' transitions, while the large peak at 4.9 eV is caused by E_2 transitions.

Wurtzite structure. In most wurtzite materials transitions at the E_0 edge occur from the two upper valence bands which are split by the crystal field. Both A and B are allowed for $\mathbf{E}\perp c$, while only the B component is allowed for $\mathbf{E}\|c$ (A is the lower in energy of the two). A third component C is due to transitions from the valence band split off by spin-orbit interaction, and is allowed for both polarizations.

ZnO. See Fig. 19. The spectra in Fig. 19 do not fit this pattern for two reasons: first, the crystal-field

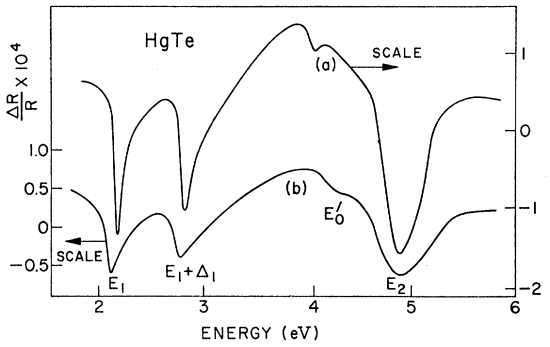

FIG. 18. Thermoreflectance spectrum of HgTe at (a) liquid-nitrogen temperature and (b) room temperature.

splitting is larger than the spin-orbit splitting, and second, the spin-orbit splitting is negative, i.e., the Γ_{9v} and $\Gamma_{7v}{}^u$ levels are reversed.[43] Taking the peaks as being representative of the edge positions, we obtain values of 3.364, 3.378, and 3.419 eV at a temperature of approximately 80°K. Thus the A-B and A-C splittings are 14 and 55 meV, respectively. The values from reflectance measurements[43] are 8 and 48 meV. The discrepancy probably lies in estimating the position of the A peak; since it is almost masked by the very large B peak, our spectral resolution of ~4 meV was probably insufficient to yield the correct shape. This structure was seen only at 80°K; no structure was observed at higher energies.

CdS. See Fig. 20. At 80°K, the A, B, and C lines are all well resolved and obey the usual wurtzite selection rules discussed above. A-B and A-C splittings of 16 and 75 meV, respectively, are obtained from peak positions of 2.544, 2.560, and 2.619 eV. Reflectance measurements by Thomas and Hopfield[44] gave similar peak positions and splittings of 15 and 72 meV at 77°K. The small structure lying ~30 meV below the lowest

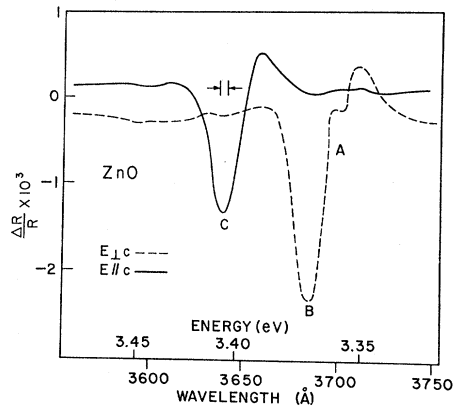

FIG. 19. Thermoreflectance spectrum of ZnO at liquid-nitrogen temperature.

[43] J. E. Rowe, M. Cardona, and F. H. Pollak, Solid State Commun. 6, 239 (1968), and references therein.
[44] D. G. Thomas and J. J. Hopfield, Phys. Rev. 116, 573 (1959).

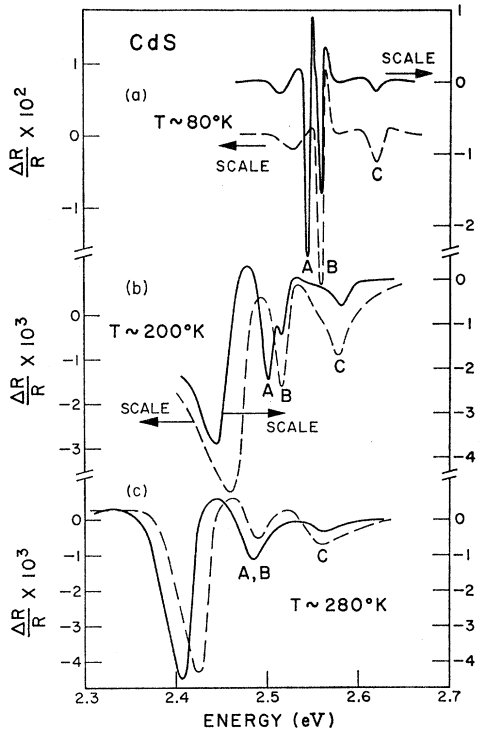

FIG. 20. Thermoreflectance spectrum of hexagonal CdS at (a) liquid-nitrogen temperature, (b) acetone-and-dry-ice temperature, and (c) room temperature.

energy peak for both $\mathbf{E}\perp c$ and $\mathbf{E}\|c$ is possibly due to a bound exciton. However, back-surface reflection effects would be expected in this case because the sample was a thin vapor-grown platelet having natural, parallel faces, and the back surface was not ground.

At ~200°K the A and B peaks are beginning to merge as a result of their broadening, but the peak separations are still similar to the 80°K values. The peak below the edge is relatively much larger than it was at 80°K, and is now clearly caused by back-surface reflection; interference fringes were observed on its low-energy side. At room temperature the A and B peaks are no longer individually distinguishable. The spectrum of Lange and Henrion[17] taken at ~330°K is quite different from that in Fig. 20 for $T\sim280$°K; the C peak did not appear, and they attribute positive peaks to A and B transitions, although the back-surface reflection is negative.

At all temperatures the C peak was larger for $\mathbf{E}\|c$ than for $\mathbf{E}\perp c$. Similar results were obtained in electroreflectance measurements[4,45]; this will be discussed further in Sec. V. Some evidence of higher gaps was seen at ~5.0 and 5.5 eV, probably corresponding to A and B transitions of type E_1, but was small and not consistently reproducible on different samples.

CdSe. See Fig. 21. Data were taken only at room temperature for this compound. The direct edge E_0 and its split-off component $E_0+\Delta_0$ occur around 2 eV; A-B and A-C splittings of 30 and 430 meV were measured from the peak positions, comparing favorably with electroreflectance results. At 3.7 eV a peak is seen for $\mathbf{E}\|c$ (a shoulder for $\mathbf{E}\perp c$) which does not correspond to any previously observed transitions. The E_1 transitions give four components[46] in the optical structure: A_1, A_2, B_1, and B_2, the first two of these being allowed for $\mathbf{E}\perp c$ only. The positions of the peaks agree well with previous reflectance[46,47] and electroreflectance data, although the B splitting is not fully resolved.

V. DISCUSSION

In order to compare our results with the theory outlined in Sec. II, we have applied a Kramers-Kronig analysis to InSb, CdTe, and Si. These materials were chosen as being representative of their periodic-table group, and also because the large spin-orbit splittings of the first two enabled the line shapes of doublet peaks to be well separated.

The thermoreflectance data of InSb show E_1 (nega-

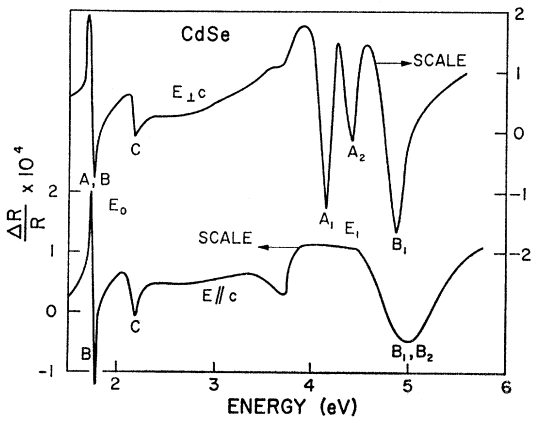

FIG. 21. Thermoreflectance spectrum of CdSe at room temperature.

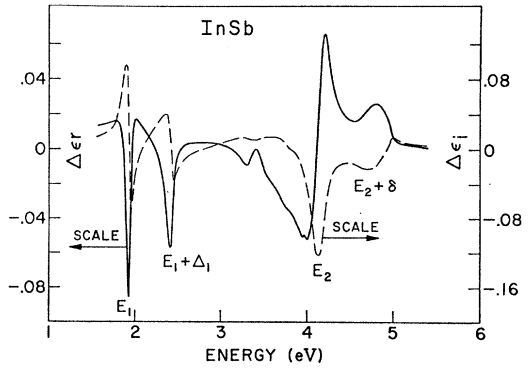

FIG. 22. $\Delta\epsilon_r$(—) and $\Delta\epsilon_i$(- - -) for InSb as obtained from the Kramers-Kronig analysis of the data in Fig. 12(a).

[45] E. Gutsche and H. Lange, Phys. Status Solidi **22**, 229 (1967).
[46] M. Cardona, Solid State Commun. **1**, 109 (1963).
[47] M. Cardona and G. Harbeke, Phys. Rev. **137**, A1467 (1965).

tive) peaks which are asymmetric; their low-energy side is steeper than the high-energy side. This shape can also be seen in the E_1 peaks of AlSb, GaSb, InAs, and HgTe. The Kramers-Kronig analysis of the data in Fig. 12 yields the changes in the optical constants $\Delta\epsilon_r$ and $\Delta\epsilon_i$ as a function of photon energy; the results at low temperatures are shown in Fig. 22. The real part $\Delta\epsilon_r$ shows quite symmetric peaks for E_1 and $E_1+\Delta_1$, while E_2 is a dispersive shape approximately symmetric about the abscissa. $\Delta\epsilon_i$ yields dispersive shapes for E_1 and $E_1+\Delta_1$ and predominantly negative peaks for E_2 and $E_2+\delta$.

It is possible to interpret the experimental line shapes of the E_1 and $E_1+\Delta_1$ peaks in terms of the shapes in Fig. 2 for M_1 critical points by mixing gap shift (with $d\omega_0/dT<0$, as in Fig. 2) and broadening spectra with roughly equal weights. While the possibility of such mixing cannot be excluded *a priori*, the broadening contribution is expected to be considerably smaller than the shift contribution, as indicated in Sec. II. However, we can exclude any significant contribution of broadening modulation to the E_1 and $E_1+\Delta_1$ peaks of Fig. 12 by comparing them with the corresponding wavelength-modulation spectra[13] shown in Fig. 23; the line shapes of the wavelength- and temperature-modulation spectra are essentially the same. Under these circumstances we must attribute the line shapes of the E_1 and $E_1+\Delta_1$ peaks of Fig. 22 to exciton interaction as discussed in Sec. II, and a mixture of the M_1 and M_2 line shapes is expected.

The E_0' and $E_0'+\Delta_0'$ structure in Fig. 22 is too weak for any line-shape considerations. The strong E_2 peak can be explained with either shift and broadening modulation at M_2 one-electron critical points, or only with shift modulation at M_2 critical points with exciton interaction. Since we believe shift modulation to be dominant, we prefer the latter interpretation.

Figure 24 shows the energy-derivative spectra of

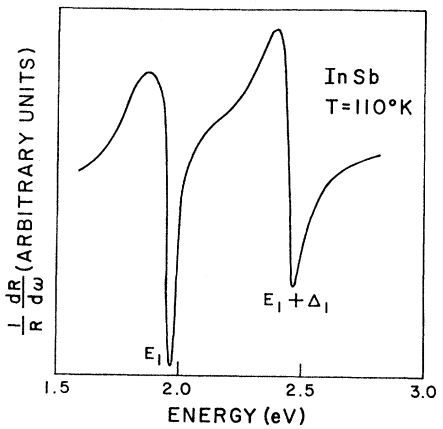

FIG. 23. Wavelength-modulated reflectance spectrum of InSb at a temperature of 110°K (see Ref. 14).

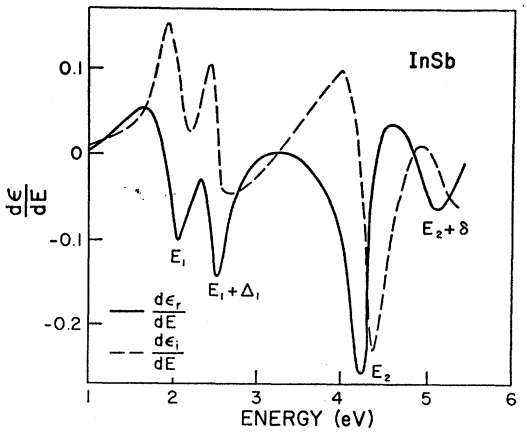

FIG. 24. The derivative of ϵ_r(—) and ϵ_i(- - -) with respect to $E=\hbar\omega$, calculated from the band structure of InSb derived by the $\mathbf{k}\cdot\mathbf{p}$ method (see Ref. 48).

InSb calculated by Higginbotham and Shaklee[48] from the one-electron band structure obtained by the $\mathbf{k}\cdot\mathbf{p}$ method. Since the temperature coefficients of the gaps are all approximately equal, the gross features of Fig. 24 should be comparable with those of Fig. 22. This conclusion is borne out by our experiment; line shapes differ of course, since the band calculations do not take into account exciton effects.

The Kramers-Kronig analysis of the low-temperature data for CdTe is shown in Fig. 25. The E_0-peak shape also requires either shift and broadening contributions to the one-electron spectra or gap-shift modulation of an excitonic spectrum. For the reasons detailed above, we believe that the shape is the result of an M_0 critical point plus exciton interaction. The E_1 peaks are similar to those in InSb, but are less well defined. The peak appearing above 5 eV is probably due to E_0' transitions;

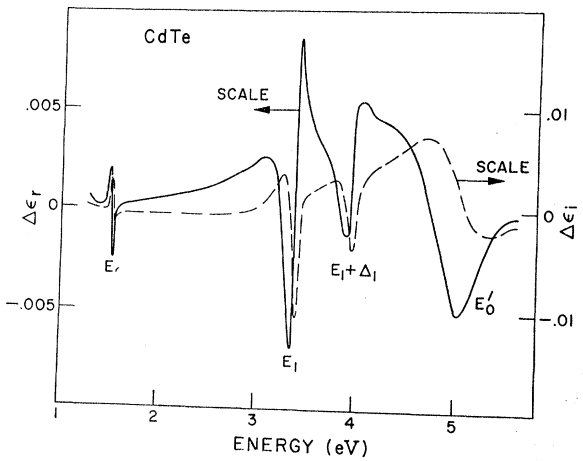

FIG. 25. $\Delta\epsilon_r$(—) and $\Delta\epsilon_i$(- - -) for CdTe as obtained from the Kramers-Kronig analysis of the data in Fig. 16(a).

[48] C. W. Higginbotham and K. L. Shaklee (private communication).

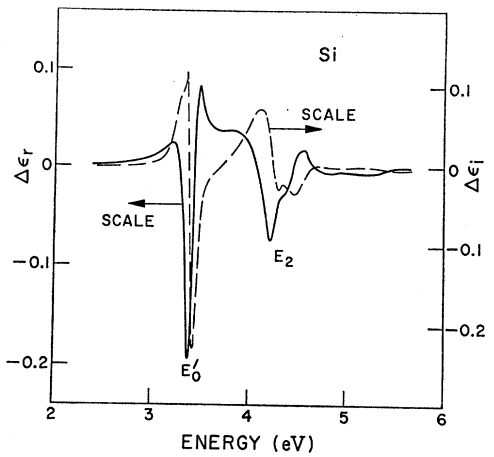

FIG. 26. $\Delta\epsilon_r$(—) and $\Delta\epsilon_i$(- - -) for Si as obtained from the Kramers-Kronig analysis of the data in Fig. 5(a).

the high noise and stray-light levels in this spectral region are responsible for the broad and vague shape shown.

There has been doubt for some time about which transitions are responsible for the optical structure in the reflectance, electroreflectance, etc., of Si at 3.4 eV.[3] Measurements on $Ge_{1-x}Si_x$ alloys[49,50] indicate that E_0' and E_1 are almost degenerate at this energy in Si. A Kramers-Kronig analysis of the thermoreflectance data is shown in Fig. 26. The doublet in the 3.4-eV structure has already been commented on in Sec. IV. From Fig. 26 it appears that the large peak is predominantly due to an M_1 critical point with exciton interaction, while the lower-energy part is possibly due to an M_0 critical point with exciton interaction. The peak above 4 eV is seen from the low-temperature data to be due to an M_1 critical point at 4.3 eV and an M_2 critical point at 4.5 eV, both involving exciton interaction; these critical points therefore probably occur at low-symmetry critical points near X and at Σ, U, etc., as mentioned in Sec. II.

While the exciton binding energy at the E_0 edge becomes greater than the broadening parameter, discrete exciton states can exist, as was pointed out in Sec. II. This is the case for three of the materials that we have measured, i.e., ZnO, ZnS, and CdS. At the E_0 edge the contribution of the change in ϵ_i to the modulation spectrum is small, and hence the shape of $\Delta R/R$ should be similar to that of $d\epsilon_r/d\omega$. Comparing $d\epsilon_r/d\omega$ and $d\epsilon_r/d\Gamma$ in Fig. 3 with $\Delta R/R$ in Figs. 13, 19, and 20, we see that in all cases the shape is well represented by $d\epsilon_r/d\omega$ with only small contributions from broadening modulation and/or asymmetric broadening.

Using the quasicubic model,[44] we calculate $\Delta_0=62$ meV and $\Delta_c=29$ meV for CdS at 80°K from the splittings of the A, B, and C peaks at the E_0 edge. We then calculate the relative intensities of the three peaks for the two directions of polarization used experimentally, setting the intensity of the A peak for $\mathbf{E}\perp c$ equal to 1. The results are shown in Table I. The heights of the experimental peaks were estimated from Fig. 20 ($T\sim 80$°K), taking the background as an arbitrary "zero line," and are also shown in Table I, again setting the value for A ($\mathbf{E}\perp c$) equal to 1. It can be seen that there is good agreement for the ratio ($\mathbf{E}\|c$):($\mathbf{E}\perp c$) for all three peaks. The agreement is also good for the A:B ratios, but not for A:C or B:C. The C peaks are expected to be of lower height than predicted by this theory since the levels involved are within the interband continuum of the A and B transitions.

TABLE I. Theoretical and experimental values of the intensities of the A, B, and C excitons in CdS, using the experimental values of the A-B and A-C splittings. The values of $I_\perp(A)$(theor) and $I_\perp(A)$(expt) have both been set equal to unity (see Sec. V).

Peak	$I_\perp$ (theor)	$I_\perp$ (expt)	$I_\parallel$ (theor)	$I_\parallel$ (expt)	$I_\parallel/I_\perp$ (theor)	$I_\parallel/I_\perp$ (expt)
A	1.00	1.00	0	0	0	0
B	0.57	0.65	0.86	0.88	1.50	1.36
C	0.43	0.09	1.12	0.19	2.60	2.1

No attempt was made to fit the experimental results to the theoretical line shapes in Fig. 2, since the degree of mixing of the M_r and M_{r+1} critical-point line shapes is not yet known.

VI. CONCLUSIONS

The results that we have shown here, in association with those of wavelength modulation, present strong evidence for the existence of electron-hole interactions at M_1 and M_2 interband critical points, besides at M_0 critical points. The existence of so-called hyperbolic excitons has been postulated previously,[51] but never demonstrated to any degree of certainty.[13] We have shown that the technique of thermoreflectance under certain conditions is equivalent to wavelength modulation and is thus capable of identifying the type of critical point involved in an interband transition. Since the sample surface is not covered in any way, the method can be extended into the vacuum ultraviolet, as has been demonstrated by Scouler.[19] In order to clarify the structure when peaks are close together (e.g., small spin-orbit splittings), it is necessary to cool the sample below liquid-nitrogen temperatures for many of the materials discussed previously; this procedure would be facilitated by depositing a thin film of the material (epitaxial if possible) directly onto the heat sink, ensuring a good thermal contact and a small heat input.

Further quantitative fitting of theory and experiment awaits detailed calculations on the effect of electron-hole interaction on interband transitions.

[49] J. Tauc and A. Abraham, J. Phys. Chem. Solids **20**, 190 (1961).

[50] J. S. Kline, M. Cardona, and F. H. Pollak, Helv. Phys. Acta (to be published).

[51] M. Cardona and G. Harbeke, Phys. Rev. Letters **8**, 90 (1962).